Highly turbulent solutions of the Lagrangian-averaged Navier-Stokes α model and their large-eddy-simulation potential

Jonathan Pietarila Graham,[1,2] Darryl D. Holm,[3,4] Pablo D. Mininni,[1,5] and Annick Pouquet[1]
[1]*National Center for Atmospheric Research, P. O. Box 3000, Boulder, Colorado 80307, USA*
[2]*Max-Planck-Institut für Sonnensystemforschung, 37191 Katlenburg-Lindau, Germany*[n1]
[3]*Department of Mathematics, Imperial College London, London SW7 2AZ, United Kingdom*
[4]*Computer and Computational Science Division, Los Alamos National Laboratory, Los Alamos, New Mexico 87545, USA*
[5]*Departamento de Física, Facultad de Ciencias Exactas y Naturales, Universidad de Buenos Aires, Ciudad Universitaria, 1428 Buenos Aires, Argentina*

(Received 15 April 2007; revised manuscript received 6 August 2007; published 14 November 2007)

We compute solutions of the Lagrangian-averaged Navier-Stokes α- (LANS α) model for significantly higher Reynolds numbers (up to $\mathrm{Re}\approx 8300$) than have previously been accomplished. This allows sufficient separation of scales to observe a Navier-Stokes inertial range followed by a second inertial range specific to the LANS α model. Both fully helical and nonhelical flows are examined, up to Reynolds numbers of ~ 1300. Analysis of the third-order structure function scaling supports the predicted l^3 scaling; it corresponds to a k^{-1} scaling of the energy spectrum for scales smaller than α. The energy spectrum itself shows a different scaling, which goes as k^1. This latter spectrum is consistent with the absence of stretching in the subfilter scales due to the Taylor frozen-in hypothesis employed as a closure in the derivation of the LANS α model. These two scalings are conjectured to coexist in different spatial portions of the flow. The l^3 $[E(k)\sim k^{-1}]$ scaling is subdominant to k^1 in the energy spectrum, but the l^3 scaling is responsible for the direct energy cascade, as no cascade can result from motions with no internal degrees of freedom. We demonstrate verification of the prediction for the size of the LANS α attractor resulting from this scaling. From this, we give a methodology either for arriving at grid-independent solutions for the LANS α model, or for obtaining a formulation of the large eddy simulation optimal in the context of the α models. The fully converged grid-independent LANS α model may not be the best approximation to a direct numerical simulation of the Navier-Stokes equations, since the minimum error is a balance between truncation errors and the approximation error due to using the LANS α instead of the primitive equations. Furthermore, the small-scale behavior of the LANS α model contributes to a reduction of flux at constant energy, leading to a shallower energy spectrum for large α. These small-scale features, however, do not preclude the LANS α model from reproducing correctly the intermittency properties of the high-Reynolds-number flow.

DOI: 10.1103/PhysRevE.76.056310 PACS number(s): 47.27.ep, 47.27.E−, 47.27.Jv, 47.50.−d

I. INTRODUCTION

Since the degrees of freedom for high-Reynolds-number (Re) turbulence, such as can be encountered in geophysical and astrophysical flows, can be very large, the implementation of their numerical modeling can easily exceed technological limits for computations. Furthermore, since truncation of the omitted scales removes important physics, e.g., of multiscale interactions, the only approach to a numerical study of such flows is to employ subgrid modeling of those scales. This is frequently accomplished with large eddy simulations (LESs); see [1–3] for recent reviews. This is of importance for geophysical, astrophysical, and engineering applications and can have consequences for meteorological [4] and climate prediction simulations [5], for instance. While realistic Reynolds numbers will remain out of reach for the foreseeable future, subgrid modeling can be an extremely useful tool in the computation of simulations for such applications.

The incompressible Lagrangian-averaged Navier-Stokes equations (LANS α, α model, or also the viscous Camassa-Holm equation) [6–11] is one possible subgrid model. It can be derived, for instance, by temporal averaging applied to Hamilton's principle (where Taylor's frozen-in turbulence hypothesis is applied as the closure, and also as the only approximation of the derivation) [12–14]. For this reason, the momentum-conservation structure of the equations is retained. For scales smaller than the filter width, the LANS α model reduces the steepness of steep gradients of the Lagrangian mean velocity and limits how thin vortex tubes become as they are transported (the effect on larger length scales is negligible) [9]. The α model may also be derived by smoothing the transport velocity of a material loop in Kelvin's circulation theorem [11]. Consequently, there is no attenuation of resolved circulation, which is important for many engineering and geophysical flows where accurate prediction of circulation is highly desirable. The LANS α model has previously been compared to direct numerical simulations (DNSs) of the Navier-Stokes equations at modest Taylor Reynolds numbers ($R_\lambda\approx 72$ [15], $R_\lambda\approx 130$ [9], and $R_\lambda\approx 300$ [16]). The LANS α model was compared to a dynamic eddy viscosity LES in three-dimensional (3D) isotropic turbulence under two different forcing functions ($R_\lambda\approx 80$ and 115) and for decaying turbulence with initial conditions peaked at a low wave number ($R_\lambda\approx 70$) and at a moderate wave number ($R_\lambda\approx 220$) [17]. In these comparisons, the LANS α model was preferable in that it demonstrated correct alignment between eigenvectors of the sub-

grid stress tensor and the eigenvectors of the resolved stress tensor and vorticity vector. The LANS α and a related regularization, the Leray model, were contrasted with a dynamic mixed (similarity plus eddy viscosity) model in a turbulent mixing shear layer ($\mathrm{Re}\approx 50$) [18,19]. The LANS α model, with relatively high subfilter resolutions, was the most accurate of these three LESs tested at this moderate Re, but it was found that the effects of numerical contamination can be strong enough to lose most of this potential. This could pose some limitations on its practical use. Quantifying those limitations is one of the goals of this present work. We will also find in this study that, even with sufficient subfilter resolution, the LANS α model fails to represent all the neglected physics in a more turbulent regime (higher Re).

The α model also describes an incompressible second-grade non-Newtonian fluid (under a modified dissipation) [11]. In this interpretation, α is a material parameter which measures the elastic response of the fluid. Either from this standpoint, from its status as a regularization of the Navier-Stokes equations, or, independently of any physically motivation, as a set of partial differential equations with proven unique regular solutions, we may analyze the LANS α model without any LES considerations. Analyzing inertial-range scaling for the LANS α model for moderate and large α, as well as identifying different scalings at scales larger and smaller than α, is another of the goals of this work. In this context we also study the numerical resolution requirements to obtain well-resolved solutions of the LANS α model (i.e., grid-independent solutions) which lead to a verification of the predictions of the size of the attractor in the LANS α model [11,20]. Section II presents the LANS α model, our numerical experiments, and technique. In Sec. III we analyze inertial-range scaling for the LANS α model. In Sec. IV we determine the numerical resolution requirements to obtain well-resolved solutions of the LANS α model. In Sec. V we address the LES potential of the LANS α model by comparing α model simulations to a 256^3 DNS ($\mathrm{Re}\approx 500$, $R_\lambda \approx 300$), a 512^3 DNS ($\mathrm{Re}\approx 670$, $R_\lambda \approx 350$), a 512^3 DNS ($\mathrm{Re}\approx 1300$, $R_\lambda \approx 490$), a 1024^3 DNS ($\mathrm{Re}\approx 3300$, $R_\lambda \approx 790$), and a 2048^3 DNS ($\mathrm{Re}\approx 8300$, $R_\lambda \approx 1300$). (The $\mathrm{Re}\approx 3300$ simulation has been previously described in a study of the imprint of large-scale flows on local energy transfer [21,22].) In Sec. VI, we compare and contrast in more detail LANS α solutions with a DNS at $\mathrm{Re}\approx 3300$. Finally, in Sec. VII we summarize our results, present our conclusion, and propose future directions of investigation.

II. TECHNIQUE

We consider the incompressible Navier-Stokes equations for a fluid with constant density,

$$\partial_t v_i + v_j \partial_j v_i = -\partial_i p + \nu \partial_{jj} v_i + F_i,$$

$$\partial_i v_i = 0, \tag{1}$$

where v_i denotes the component of the velocity field in the x_i direction, p the pressure divided by the density, ν the kinematic viscosity, and F_i an external force that drives the turbulence (in all results, the time t is expressed in units of the eddy-turnover time). The LANS α equations [6–11] are given by

$$\partial_t v_i + u_j \partial_j v_i + v_j \partial_i u_j = -\partial_i \pi + \nu \partial_{jj} v_i + F_i,$$

$$\partial_i v_i = \partial_i u_i = 0, \tag{2}$$

where u_i denotes the filtered component of the velocity field and π the modified pressure. Filtering is accomplished by the application of a normalized convolution filter $L: f \mapsto \bar{f}$ where f is any scalar or vector field. By convention, we define $u_i \equiv \bar{v}_i$. We choose as our filter the inverse of a Helmholtz operator, $L = \mathcal{H}^{-1} = (1 - \alpha^2 \partial_{kk})^{-1}$. Therefore, $\mathbf{u} = g_\alpha \otimes \mathbf{v}$ where g_α is the Green's function for the Helmholtz operator, $g_\alpha(r) = \exp(-r/\alpha)/(4\pi\alpha^2 r)$ (i.e., the well-known Yukawa potential), or in Fourier space $\hat{\mathbf{u}}(k) = \hat{\mathbf{v}}(k)/(1 + \alpha^2 k^2)$.

We solve Eqs. (1) and (2) using a parallel pseudospectral code [23,24] in a three-dimensional cube with periodic boundary conditions. In most of the runs, we employ a Taylor-Green forcing [25],

$$F = \begin{bmatrix} \sin k_0 x \cos k_0 y \cos k_0 z \\ -\cos k_0 x \sin k_0 y \cos k_0 z \\ 0 \end{bmatrix} \tag{3}$$

(generally, with $k_0 = 2$), and employ dynamic control [26] to maintain a nearly constant energy with time. This expression Eq. (3) is not a solution of Euler's equations, and as a result small scales are generated quickly when the fluid is stirred with this forcing. The resulting flow models the fluid between counter-rotating cylinders [27] and has been widely used to study turbulence, including studies in the context of the generation of magnetic fields through dynamo instability [28]. We also consider some runs with random and Arn'old-Childress-Beltrami (ABC) [22] forcing. We define the Taylor microscale as $\lambda = 2\pi\sqrt{\langle v^2 \rangle / \langle \omega^2 \rangle}$, and the mean velocity fluctuation as $v_{\mathrm{rms}} = [2\int_0^\infty E(k)dk]^{1/2}$. The Taylor microscale Reynolds number is defined by $R_\lambda = v_{\mathrm{rms}}\lambda/\nu$ and the Reynolds number based on a unit length is $\mathrm{Re} = v_{\mathrm{rms}} \times 1/\nu$.

III. INERTIAL RANGE SCALING OF THE LANS α MODEL

A. l^3 scaling of third-order structure function derived from the Kármán-Howarth theorem for the LANS α model

For the LANS α model, the $H^1_\alpha(u)$ norm is the quadratic invariant to be identified with the energy,

$$\frac{dE_\alpha}{dt} = -2\nu\Omega_\alpha, \tag{4}$$

where

$$E_\alpha = \frac{1}{D}\int_D \frac{1}{2}(\mathbf{u} - \alpha^2 \nabla^2 \mathbf{u}) \cdot \mathbf{u}\, d^3x = \frac{1}{D}\int_D \frac{1}{2}\mathbf{v} \cdot \mathbf{u}\, d^3x \tag{5}$$

and

$$\Omega_\alpha = \frac{1}{D}\int_D \frac{1}{2}\boldsymbol{\omega}\cdot\bar{\boldsymbol{\omega}}\, d^3x. \tag{6}$$

As usual, we define the (omnidirectional) spectral energy density $E_\alpha(k)$ from the relation

$$E_\alpha = \int_0^\infty \oint E_\alpha(\mathbf{k}) d\sigma\, d\mathbf{k} = \int_0^\infty E_\alpha(k) dk, \tag{7}$$

where $\oint d\sigma$ represents integration over the surface of a sphere. The α model possesses a theorem corresponding to the Kármán-Howarth theorem [29] for the Navier-Stokes equations and, as in the Navier-Stokes case, scaling of the inertial range energy spectra may be derived from it [30]. We summarize here the dimensional analysis argument for the LANS α inertial range scaling that follows from this theorem, beginning from Eq. (3.8) in Ref. [30]. We use the short notation $v_i \equiv v_i(\mathbf{x})$, $u_i' \equiv u_i'(\mathbf{x}', t)$, and $\mathbf{r} \equiv \mathbf{x}' - \mathbf{x}$. In the statistically isotropic and homogeneous case, without external forces and with $\nu = 0$, taking the dot product of Eq. (2) with u_j', we can obtain the equation

$$\partial_t \mathcal{Q}_{ij} = \frac{\partial}{\partial_{r^m}}(\mathcal{T}_{ij}^m - \alpha^2 \mathcal{S}_{ij}^m). \tag{8}$$

The trace of this equation is the Fourier transform of the detailed energy balance for the LANS α model.

$$\mathcal{Q}_{ij} = \langle v_i u_j' + v_j u_i' \rangle \tag{9}$$

is the second-order correlation tensor while

$$\mathcal{T}_{ij}^m = \langle (v_i u_j' + v_j u_i' + v_i' u_j + v_j' u_i) u^m \rangle \tag{10}$$

and

$$\mathcal{S}_{ij}^m = \langle (\partial_m u_l \partial_i u_l) u_j' + (\partial_m u_l \partial_j u_l) u_i' + (g_\alpha \otimes \tau_j'^m) v_i + (g_\alpha \otimes \tau_i'^m) v_j \rangle \tag{11}$$

are the third-order correlation tensors for the LANS α model and τ_i^j is the subfilter scale stress tensor. For $\alpha = 0$ this reduces to the well-known relation derived by Kármán and Howarth. The energy dissipation rate for the LANS α model, ε_α, satisfies $\varepsilon_\alpha \propto \partial_t \mathcal{Q}_{ij}$. By dimensional analysis in Eq. (8) we arrive at

$$\varepsilon_\alpha \sim \frac{1}{l}\left(v u^2 + \frac{\alpha^2}{l^2} u^3\right). \tag{12}$$

For large scales such that $l \gg \alpha$, the second right-hand term is ignored, $\mathbf{u} \approx \mathbf{v}$, $\varepsilon_\alpha \approx \varepsilon$, and we arrive at the scaling of the four-fifths law $\langle [\delta v_\parallel(l)]^3 \rangle \sim \varepsilon l$ [31]. Here, $\delta v_\parallel(l) \equiv [\mathbf{v}(\mathbf{x}+\boldsymbol{l}) - \mathbf{v}(\mathbf{x})] \cdot \boldsymbol{l}/l$ is the longitudinal increment of $\mathbf{v}$. The four-fifths law expresses that the third-order longitudinal structure function of $\mathbf{v}$, $S_3^v \equiv \langle (\delta v_\parallel)^3 \rangle$, is given in the inertial range in terms of the mean energy dissipation per unit mass ε by

$$S_3^v = -\frac{4}{5}\varepsilon l, \tag{13}$$

or, equivalently, that the flux of energy across scales in the inertial range is constant. We also obtain the Kolmogorov 1941 [32–34] (K41) energy spectrum, $E(k)k \sim v^2 \sim \varepsilon^{2/3} l^{2/3}$, or, equivalently,

$$E(k) \sim \varepsilon^{2/3} k^{-5/3}. \tag{14}$$

For small scales such that $l \ll \alpha$, however, $v \sim \alpha^2 l^{-2} u$ and both right-hand terms are equivalent in Eq. (12), and our scaling law becomes

$$S_3^u \equiv \langle [\delta u_\parallel(l)]^3 \rangle \sim \varepsilon_\alpha \alpha^{-2} l^3. \tag{15}$$

Note that this scaling differs in a substantial way from the Kolmogorov scaling ($\sim l$). For our small-scale energy spectrum we then have

$$E_\alpha(k)k \sim uv \sim \varepsilon_\alpha^{2/3} \alpha^{2/3}, \tag{16}$$

where we used $u \sim \alpha^{-2} l^2 v$. The energy spectrum for scales smaller than α is then

$$E_\alpha(k) \sim \varepsilon_\alpha^{2/3} \alpha^{2/3} k^{-1}. \tag{17}$$

This spectrum can also be derived from phenomenological arguments originally introduced by Kraichnan [35], and it differs from the Navier-Stokes spectrum due to the fact that the fluid is advected by the smoothed velocity $\mathbf{u}$, which does not directly correspond to the conserved energy E_α [11].

We test this prediction for LANS α scaling at a resolution of 256^3 ($\nu = 1.2 \times 10^{-4}$) by moving both the forcing ($k_0 = 1$) and α ($k_\alpha \equiv 2\pi/\alpha = 3$) to large scales in order to increase the number of resolved scales for which $k\alpha > 1$. In so doing, we are assuming that the scaling for large α is the same as for small α and large k (for evidence to this effect, see [36]). Confirmation as given by Eq. (15) is presented in Fig. 1 where we plot S_3^u as a function of l [by convention, we plot $S_3^u = \langle |\delta u_\parallel(l)|^3 \rangle$ to reduce cancellation in the statistics]. The scales identified with an inertial range $k \in [6, 10]$ are marked by vertical dashed lines and the predicted scaling, l^3, is indicated by a solid line. We fit a scaling exponent $[S_3^u(l) \sim l^{\zeta_3^u}]$

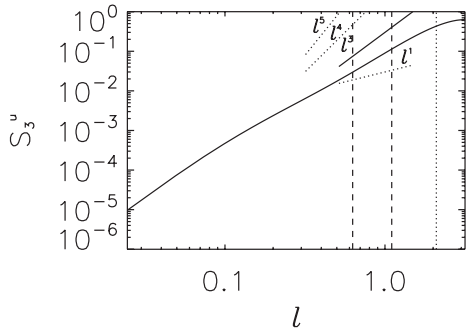

FIG. 1. Third-order longitudinal structure function of the smoothed velocity field $\mathbf{u}$, S_3^u, versus l for large α in the LANS α model ($\alpha = 2\pi/3$ indicated by the vertical dotted line). The scales identified with an inertial range are marked by vertical dashed lines and the scaling predicted by Eq. (15), l^3, is indicated by a solid line. The fitted scaling exponent ζ_3^u $[S_3^u(l) \sim l^{\zeta_3^u}]$ is found to be $\zeta_3^u = 2.39 \pm 0.04$. This is more consistent with the scaling given by Eq. (15) than K41 scaling, l^1 Eq. (13), or other proposed LANS α scalings (indicated by dotted lines, see text).

and find $\zeta_3^u = 2.39 \pm 0.04$. This is significantly steeper than the classical Kolmogorov scaling given by Eq. (13); it can thus be viewed as more consistent with the scaling given by Eq. (15). It is also more consistent with l^3 than with other possible LANS α scalings: under the assumption that the turnover time scale of eddies of size $\sim l$ is determined by the unsmoothed velocity $\mathbf{v}$, we find $S_3^u(l) \sim l^5$, and if it is determined by $\sqrt{\mathbf{v}\cdot\mathbf{u}}$, we find $S_3^u(l) \sim l^4$ (see, e.g., Refs. [16,36–38]). The observed scaling corresponds to none of these cases, and is actually closer to an evaluation of the turnover time t_l at the scale l given by $t_l \sim l/u_l$ [with $S_3^u(l) \sim l^3$]. Note that for the 2D LANS α model, however, it is the case that the scaling is determined by the unsmoothed velocity $\mathbf{v}$ [36]. We note that this is one of many differences between the 2D and 3D cases (e.g., ideal invariants and cascades). Another difference, which we shall show in Sec. VI, is that in 2D vorticity structures decrease in scale as α increases, while in 3D there is a change in aspect ratio with structures getting both shorter and fatter. This may, in fact, be related to the shallower LANS α energy spectrum for $k\alpha > 1$, which we show in Sec. VI. While differences are observed between the scaling shown in Fig. 1 and Eq. (15), the error bars deny a K41 scaling (as well as the l^4 and l^5 scalings) at scales smaller than α. We believe the discrepancy between the observed and predicted scalings might be due to lack of ability to resolve properly the inertial range at subfilter scales. We have less than a decade of inertial range and only 256^3 points for the statistics. As more computational resources become available, this scaling should be reexamined.

B. Subdominance of the k^{-1} energy spectrum and rigid-body motions

As a consequence of the LANS α model's Taylor frozen-in hypothesis closure, scales smaller than α can phase-lock into coherent structures and be swept along by the larger scales (see, e.g., [30]). If we assume, formally, that this "frozen-in turbulence" takes the form of "rigid bodies" in the smoothed velocity field (no stretching), we arrive at a much different spectrum than k^{-1} [Eq. (17)]. All scales smaller than α are subject to the frozen-in hypothesis and we expect to find such rigid bodies at these scales. We note that collections of rigid portions of the flow (rotating or nonrotating) reduce the total degrees of freedom (DOF) and make physical sense with the LANS α model's relation to second-grade fluids: these rigid bodies can be envisioned as polymerized portions of the fluid. As a matter of fact, in such structures all internal DOF are frozen. These rigid bodies follow as well from the consideration of the LANS α model as an initial value problem in Fourier space, for which we have $\hat{\mathbf{u}}(k) = \hat{\mathbf{v}}(k)/(1+\alpha^2 k^2)$. In the limit as α approaches infinity, all wave number (and spatial) dependence for $\bar{\mathbf{v}}$ is eliminated and the entire flow is advected by a uniform velocity field (advection without internal degrees of freedom).

For a rigid body there can be no stretching and, therefore, all the longitudinal velocity increments $\delta u_\parallel$ must be identically zero [$\delta\mathbf{u}(\boldsymbol{l}) = \boldsymbol{\Omega} \times \boldsymbol{l}$ from basic mechanics with $\boldsymbol{\Omega}$ the rotation vector, and, hence, $\delta u_\parallel(l) = \delta\mathbf{u}(\boldsymbol{l}) \cdot \boldsymbol{l}/l = 0$]. Note that

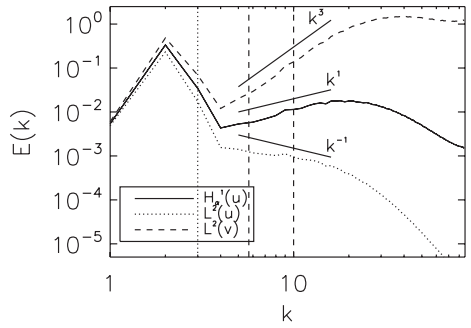

FIG. 2. Spectral energy density $E(k)$ versus wave number k for large-α LANS α solution. Here forcing ($k_0 = 1$) and α ($k_\alpha \equiv 2\pi/\alpha = 3$, vertical dotted line) are set at the largest scales to increase the number of scales for which $k\alpha > 1$. Spectra are plotted for three norms: $H_\alpha^1(u)$ norm (solid line), $L^2(u)$ norm (dotted line), and $L^2(v)$ norm (dashed line). As these last two norms are not quadratic invariants of the LANS α model, we employ the H_α^1 norm for all following results. All three spectra correspond to that derived from the assumption of rigid bodies in the smoothed velocity $\mathbf{u}$, Eq. (19). The vertical dashed lines are at the same scales as those in Fig. 1.

in the LANS α model, Eq. (2), the $v_j \partial_i u_j$ term contributes only a rotation and not a stretching of $\mathbf{u}$. Such polymerization would have two consequences. First, since there is no stretching, these rigid bodies would not contribute to the turbulent energy cascade,

$$\langle [\delta u_\parallel(l)]^3 \rangle = 0. \tag{18}$$

Second, the energy spectrum from dimensional analysis [$u^2 \sim$ const; for large α/l, $u = (1+\alpha^2/l^2)^{-1} v \sim l^2 v$, and $E_\alpha(k) k \sim uv \sim k^2$] is

$$E_\alpha(k) \sim k. \tag{19}$$

This is, in fact, the observed LANS α spectrum for $k\alpha \gg 1$ as is shown in Fig. 2. We verified that the spectrum is not the result of under-resolved runs, as is the case, e.g., in the k^2 spectrum observed in truncated Euler systems [39] or in extremely under-resolved spectral simulations of the Navier-Stokes equations. Indeed, equipartition of the energy among all modes in a truncated Euler α system should also lead to a k^2 spectrum. Along with several experiments with different viscosities and also with statistically homogeneous and isotropic forcing (not shown here), these are assurances that the observed spectrum is not a result of inadequate numerical resolution. It should be noted that this is the same computation for which the third-order structure function is shown in Fig. 1. The third-order structure function is consistent with an l^3 scaling (corresponding to a k^{-1} energy spectrum) while the spectrum itself is k^1. [Also shown in Fig. 2 are the $L^2(u) \equiv \langle u^2 \rangle/2$ and the $L^2(v) \equiv \langle v^2 \rangle/2$ norms, which (through $u \sim \alpha^2 v/k^2$ for $k\alpha \gg 1$) correspond to k^{-1} and k^3 spectra, respectively. Since the analytical properties of the LANS α solution are based on the energy balance $dE_\alpha/dt = -2\nu\Omega_\alpha$, in the $H_\alpha^1(u)$ norm, we employ this norm for all following results.] These two different scalings, l^3 and k^1, are consistent with a picture where a fluid has both rigid-body portions at scales smaller than α (wherein there is no turbulent cascade)

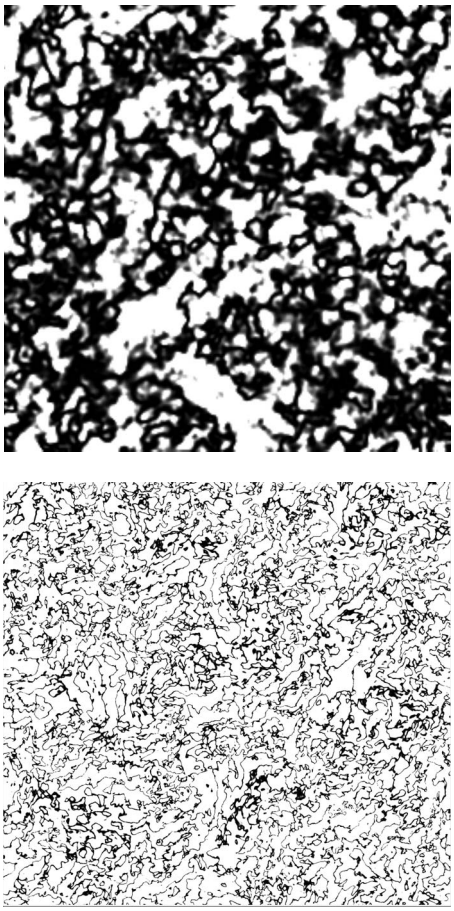

FIG. 3. Two-dimensional slice of the cubed longitudinal increment $[\delta u_{\|}(2\pi/10)]^3$ for the LANS α model and $[\delta v_{\|}(2\pi/10)]^3$ for a DNS. For all black pixels, the cubed longitudinal increment is less than 10^{-2} (approximately consistent with rigid bodies). On the top is the large-α simulation ($k_0=1$, $k_\alpha=3$, $\nu=1.2\times10^{-4}$) where the filling factor (computed over the entire 3D domain) is 0.67. On the bottom is a DNS of Navier-Stokes ($k_0=2$, $\nu=3\times10^{-4}$) where the filling factor is 0.26. Thus, a much greater portion of the flow is consistent with collections of rigid bodies for the large-α simulation.

and spatial regions between these where the cascade does take place. For the structure functions, a noncascading rigid body does not contribute to the scaling and consequently the cascading contribution, Eq. (15), dominates. The energy spectrum, however, for the limit of k very large, is dominated by the k^{+1} term, and hence the k^{-1} component is subdominant.

We further explore the validity of this picture by examining the spatial variation of the cubed longitudinal increment $[\delta v_{\|}(l)]^3$ in DNSs and $[\delta u_{\|}(l)]^3$ in the LANS α model for $\alpha/l \gg 1$, which in each case is proportional to the energy flux across a fixed scale l. (The presence of the hypothesized rigid bodies should be evident as significant portions of the flow where there is no energy flux.) In Fig. 3 we show visualizations of these quantities corresponding to $l=2\pi/10$ ($k=10$) for both the large-α LANS α simulation and a highly turbulent DNS ($k_0=2$, $\nu=3\times10^{-4}$). The scale ($k=10$) is chosen as it is in the inertial ranges of both flows. We note that, for the

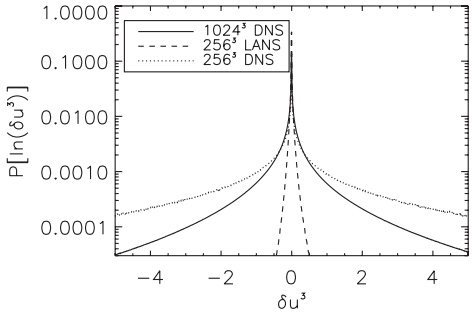

FIG. 4. PDFS of $[\delta v_{\|}(2\pi/10)]^3$ for DNS ($N=1024$, solid line), and of $[\delta u_{\|}(2\pi/10)]^3$ for the LANS α model ($N=256$, dashed line), and of the DNS downgraded to lower resolution ($N=256$, dotted line). See Fig. 3 for simulation parameters. Note that both PDFs have a slight positive asymmetry consistent with a positive dissipation rate $\varepsilon_{(\alpha)}$. The LANS α PDF is more strongly concentrated around zero, consistent with the idea that portions of the flow (at scales smaller than α) are acting as rigid bodies.

LANS α model, a significant portion of the flow is not contributing to the flux of energy to smaller scales [the filling factor for $(\delta u_{\|}(2\pi/10))^3 < 10^{-2}$ is 0.67 as compared to 0.26 for the Navier-Stokes case]. These regions can be identified as "polymerized" or "rigid bodies" in $\mathbf{u}$ and their locations are found to be robust when the l used for $[\delta u_{\|}(l)]^3$ is varied over a factor of 2. Moreover, this is highlighted in the probability distribution functions (PDFs); see Fig. 4, where we see that the LANS α PDF is more strongly concentrated around zero than that of the DNS. This is consistent with the idea that the internal DOF of large portions of the flow (at scales smaller than α) are frozen. We point out that this comparison is not a LES validation, but, rather, a comparison between the dynamics of two different fluids at similar Reynolds numbers. One flow is a well-resolved numerical solution of the Navier-Stokes equations, and the other is a well-resolved solution of the LANS α equations with large α. For this reason a reduced resolution ($N=256$) representation for the DNS (for which $N=1024$) is not depicted in Fig. 3. We have performed such a down-sampling, however, and find the filling factor is reduced even more, to 0.14, and the tails of the PDF increase over the full-resolution analysis (dotted line in Fig. 4). No inverse Helmholtz filtering, $\mathcal{H}^{-1}$, is applied to the DNS data. Note that this would amount to computing $[\delta u_{\|}(l)]^3$ in the DNS, which has no meaning in the dynamics of the Navier-Stokes equations (the energy flux is proportional to $[\delta v_{\|}(l)]^3$).

We end this section with further evidence of coexistent energy spectra, k^{-1} and k^1, in separate spatial portions of the flow. We mask out all portions of the flow that we identify with rigid bodies ($[\delta u_{\|}(2\pi/10)]^3 < 10^{-2}$, a 2D slice of which is shown in Fig. 3). The energy spectrum of the remaining portion of the flow is shown in Fig. 5 as a dashed line to be compared with the spectrum of the entire flow shown as a solid line. The operation of spatially filtering the flow before computing the spectrum serves to "smear out" the energy spectrum by convolving it with the spectrum of the filter. Deconvolution in 3D with $N=256$ is intractable and we are, therefore, unable to remove this smearing of the energy spec-

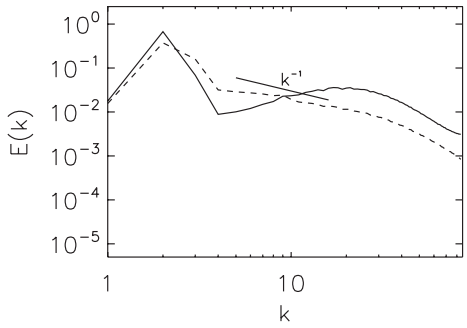

FIG. 5. Spectral energy density $E(k)$ versus wave number k for large-α LANS α solution. The solid line indicates the spectrum as given in Fig. 2 but for a single snapshot (the same as selected for Fig. 3). The dashed line indicates the spectrum wherein all portions of the flow associated with rigid bodies (a 2D slice of which is shown in Fig. 3) are removed. This provides further evidence that the flow spatially in between the rigid bodies possesses a negative power law energy spectrum (the predicted k^{-1} power law is shown as a solid line).

trum of the cascading portions of the flow. Nonetheless, after conducting what tests we could with the filtering process (not shown here), we conclude that the power law of the energy spectrum of these portions is negative and, thus, distinctly different from that of the rigid bodies.

IV. RESOLUTION REQUIREMENTS FOR GRID-INDEPENDENT LANS α SOLUTIONS: SIZE OF ATTRACTOR

It is useful to make a distinction between the quality of a subgrid model and effects arising from nonlinear interactions with discretization errors at marginal spatial resolutions (which are more characteristic of the discretization employed than of the subgrid model) [19,40,41]. Before doing this, we require an estimate for the total degrees of freedom for the LANS α attractor which as we show, unlike for the 2D case (see [36]), for the 3D case is reduced compared to Navier-Stokes. The subdominant l^3 scaling is associated with the flux of energy to small scales and thus must be used to estimate the degrees of freedom of the LANS α attractor, $n_{\mathrm{DOF}(\alpha)}$. For dissipation, the large wave numbers dominate and, therefore, combining the LANS α energy balance, Eq. (4), with its subfilter scale energy spectrum, Eq. (17), allows us to implicitly specify its dissipation wave number k_η^α by

$$\frac{\varepsilon_\alpha}{\nu} \sim \int^{k_\eta^\alpha} k^2 E_\alpha(k) dk \sim \int^{k_\eta^\alpha} k^2 \varepsilon_\alpha^{2/3} \alpha^{2/3} k^{-1} dk \sim \varepsilon_\alpha^{2/3} \alpha^{2/3} (k_\eta^\alpha)^2. \tag{20}$$

Then we have

$$k_\eta^\alpha \sim \frac{\varepsilon_\alpha^{1/6}}{\nu^{1/2} \alpha^{1/3}}. \tag{21}$$

Using the fact that the linear numerical resolution N must be proportional to the dissipation wave number ($N \geq 3k_\eta^\alpha$) and that $\mathrm{Re} \sim \nu^{-1}$, we arrive at

$$N = C_0 k_\alpha^{1/3} \mathrm{Re}^{1/2}, \tag{22}$$

or, equivalently,

$$n_{\mathrm{DOF}(\alpha)} = \frac{C_0^3}{27\alpha} \mathrm{Re}^{3/2}, \tag{23}$$

where C_0 is an unknown constant (for further details, see [11]). We verify this prediction and determine the constant C_0 through the use of a database stemming from studies in which both the free parameter α (or, equivalently, k_α) and the linear resolution N for a set of DNS flows with $\mathrm{Re} \approx 500$, 670, 1300, and 3300 are varied. In so doing, we establish the necessary numerical resolution for convergence to a grid-independent solution.

Convergence to the grid-independent solution is determined by comparison of the energy spectrum $E_\alpha(k)$ between runs with a constant filter and varying resolution. In Fig. 6(a), we make such a comparison for $\mathrm{Re} \approx 500$ ($N=256$ for the DNS) and $k_\alpha = 14$ ($N=84$, 96, 108, 128, and 192 for the LANS α model). We plot energy spectra compensated by $k^{5/3}$ so that a K41 $k^{-5/3}$ spectrum would be flat. We see, based on comparing the energy spectra at wave numbers smaller than k_α to the 192^3 LANS α spectrum, that simulations at resolutions of 96^3 and less are not converged while the one at 128^3 is. That is, except for the very small scales at the end of the dissipative range, there is very little difference between the spectra at 128^3 and at 192^3 (i.e., the solution is "grid independent"). Meanwhile, for resolutions of 96^3 and less the spectra vary greatly with resolution (i.e., they are "unresolved"). In Fig. 6(b), we collect all the results of similar studies ($\mathrm{Re} \approx 500$) in a plot of resolution N versus inverse filter width k_α. (We change N for a given α, then change α and iterate.) Pluses correspond to grid-independent solutions, $\times$'s to under-resolved solutions, and squares to "undecided" runs (i.e., those that are neither clearly resolved nor clearly under-resolved). The dashed lines represent Eq. (22) with the minimal and maximal choice of C (where $C_0 = C\mathrm{Re}^{1/2}$), that agrees with our results (i.e., $43.2 < C < 50.2$). In Fig. 7 we conduct similar studies for $Re \approx 670$. We find $49.5 < C < 51.4$ and again validate the predictive power of Eq. (22) for the necessary numerical resolution for grid-independent solutions.

The greatest utility of the prediction, however, is due to the single constant C_0 which is independent of Reynolds number. A determination of this constant can be achieved cheaply repeating this process for several runs for low and moderate Re, and determines the resolution requirement for the highest Re attainable. The ranges of acceptable constants, $C = C_0 \mathrm{Re}^{1/2}$, for the four Reynolds number flows studied are plotted versus Re in Fig. 8. A power law $C = C_0 \mathrm{Re}^\gamma$ fits our data with $\gamma = 0.54 \pm 0.14$, demonstrating the final validation of the prediction, $\gamma = 0.5$, Eq. (22). The value of the constant is found to be $C_0 = 2.0 \pm 0.2$. We made one study for the maximally helical ABC forcing at $\mathrm{Re} \approx 1600$ and $\alpha = 2\pi/25$. It is consistent with a value of $C_0 = 1.8 \pm 0.1$. We therefore conclude that the constant C_0 is not a strong function of the forcing employed or of the scale at which the system is forced. As a result, and unlike in the 2D LANS α model [36], we verify that the size of the attractor in the 3D LANS α

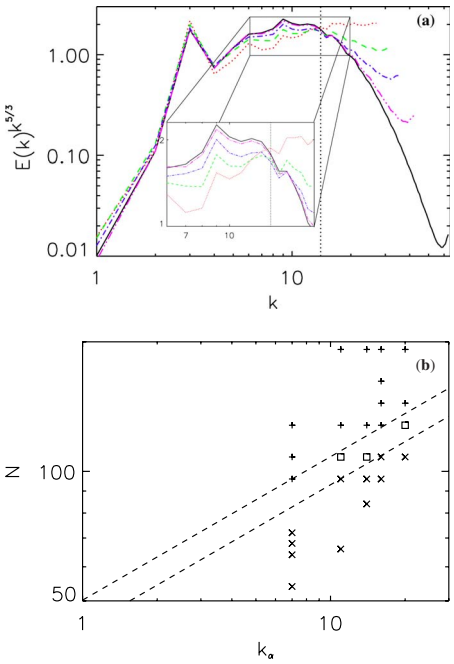

FIG. 6. (Color online) Plots for Re≈500 simulations demonstrating convergence to the grid-independent LANS α solution. (a) Average energy spectra ($t \in [20,33]$, t is time in units of eddy turnover time) compensated by K41 for LANS α simulations, $k_\alpha=14$: 192^3 (black solid), 84^3 (red dotted), 96^3 (green dashed), 108^3 (blue dash-dotted), and 128^3 (pink dash-triple-dotted). The vertical dashed line denotes k_α. Inset is a blowup near k_α where convergence can be clearly seen. The LANS α model at a linear resolution of 128^3 is approximately converged to the grid-independent solution while resolutions of 96^3 and less are clearly not. (b) The linear resolution of α model simulations, N, is plotted versus k_α. Simulations with inadequate resolution are plotted as ×'s, those with approximately grid-independent solutions as +'s, and experiments that are neither clearly resolved nor clearly unresolved as boxes. The dashed lines represent $N=Ck_\alpha^{1/3}$, indicating that a constant in the range $43.2<C<50.2$ agrees with our data. This partially confirms the prediction of Eq. (22) and provides a reliable method to determine the needed resolution for a grid-independent LANS α solution at a fixed Re.

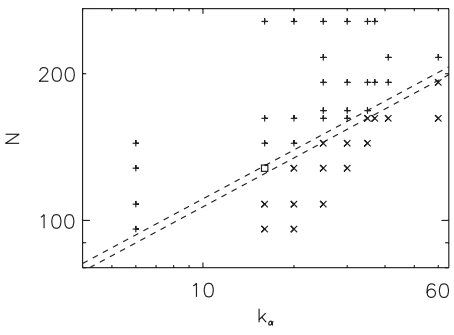

FIG. 7. As Fig. 6(b) but for Re≈670 simulations. The dashed lines represent $N=Ck_\alpha^{1/3}$, indicating that a constant in the range $49.5<C<51.4$ agrees with our data. Note also that any power law $N \propto k_\alpha^\beta$ with $0.30<\beta<0.46$ also agrees with the data.

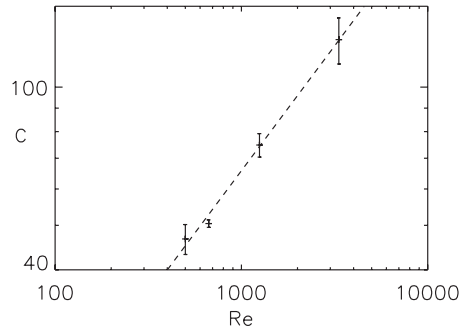

FIG. 8. Acceptable choices of $C=C_0\mathrm{Re}^{1/2}$, versus Reynolds number Re for grid-independent LANS α model. Error bars are not confidence levels, but depict the range of values consistent with our database ($N=Ck_\alpha^{1/3}$) at the four Reynolds numbers we tested. The dashed line depicts the least-squares fit with slope 0.54±0.14. This completes the validation of Eq. (22), which predicts 0.5.

model is smaller than that in the Navier-Stokes equations, which is a promising result if the LANS α equation is going to be used as a LES. However, before doing this, an assessment of the truncation errors introduced in discretized systems (as used to solve the equations numerically) and a study of the optimal choice for α to capture the properties of a DNS is needed. We consider these problems in the following section.

V. CAN THE LANS α MODEL BE CONSIDERED AS A LARGE EDDY SIMULATION?

In this section, we consider the LANS α equations as a means to an end, and consider the solutions to their discretized equations as approximations to the Navier-Stokes solutions. We seek numerical approximations of the LANS α equations that minimize the difference from a fully resolved or direct numerical solution of the Navier-Stokes equations (i.e., we analyze the behavior of LANS α solutions in the LES framework, and call here the model a LANS α LES, or in short α LES). In the LES framework, the LANS α model's turbulent stress tensor $\bar{\tau}_{ij}^{\alpha}$ is given by (see, e.g., [42])

$$\bar{\tau}_{ij}^{\alpha} = \mathcal{H}^{-1}\alpha^2(\partial_k u_i \partial_k u_j + \partial_k u_i \partial_j u_k - \partial_i u_k \partial_j u_k). \qquad (24)$$

Previous studies have not made the distinction between the grid-independent LANS α simulation and the LANS α LES, though one did study convergence to grid-independent solutions at moderate Re [19]. We find, however, a definite difference between the two approaches. We show in this section that, in fact, the LANS α model combined with truncation error yields a better fit to the DNS than the grid-independent LANS α model. The resolution that yields an optimal α LES (a terminology to be defined below) is also found to follow Eq. (22). In Sec. V A, we then address the quality and usability of the predictions of the LANS α model viewed as a LES.

A remark about nomenclature may be in order at this point. Traditionally, and for good reasons, LESs attempt to capture the large-scale properties of a flow with a huge Reynolds number, as found, e.g., in the atmosphere. In that case,

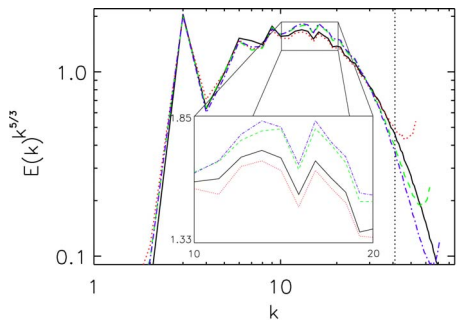

FIG. 9. (Color online) Plot of Re≈670 simulations. Average compensated energy spectra from DNS (solid black line) and LANS α simulations, $k_\alpha=41$: $N=162$ (red dotted), 192 (green dashed), and 216 (blue dash-dotted). The LANS α solution at a linear resolution of 192 is approximately converged to the grid-independent solution while a resolution of 162 is not. $N=162$ does correspond, however, more closely to the DNS spectrum. We observe, in general, that a combination of LANS α and truncation error yields the optimal α LES.

the wave number at which the DNS is truncated is, at best, in the inertial range, and it might even be in the energy-containing range, as for the atmospheric boundary layer with a Taylor Reynolds number $R_\lambda \sim 10^4$. Of a different nature are the modeling methods sometimes called quasi-DNSs. Here, the idea is to model a flow at a given, moderate Reynolds number but with an expense in computing resources less than if performing a DNS. Under-resolved DNSs fall in that category; in that case, the large scales are presumably well reproduced but the small scales are noisy. It is in that spirit that we now examine the properties of the LANS α model. We thus qualify a model as optimal in the sense of being optimal for the class of LANS α models examined herein; in order to avoid repetition, we also use the terminology of optimal α.

In Fig. 9 with $k_\alpha=41$, we plot the Re≈670 DNS spectrum (solid black line) and LANS α spectra at three different resolutions. We observe that, while the $N=162$ solution (dotted line, red online) is not converged, it is a better approximation to the DNS than the grid-independent LANS α solution. For all simulations we studied, the grid-independent LANS α solution is not the best approximation to the DNS. Another example is given in Fig. 10 where we plot the mean square spectral error normalized to make fair comparisons between large- and small-k_α results,

$$E_{\mathrm{sq}} = \frac{1}{n}\sum_{k=k_F}^{k_\alpha} \frac{[E_\alpha(k) - E(k)]^2}{E^2(k)}, \tag{25}$$

where k_F is the wave number for the forcing scale, $E(k)$ is the DNS spectrum [in the $L^2(v)$ norm], $E_\alpha(k)$ is the LANS α spectrum [in the $H^1_\alpha(u)$ norm], and n is the number of terms in the sum. These errors are calculated for spectra averaged over turbulent steady-state solutions: $t\in[16,19]$ for Re ≈670. We see that, for a given filter or a given simulation resolution, there is a local minimum in the error. This minimum is a balance between truncation errors and the approximation error due to using the LANS α method instead of the

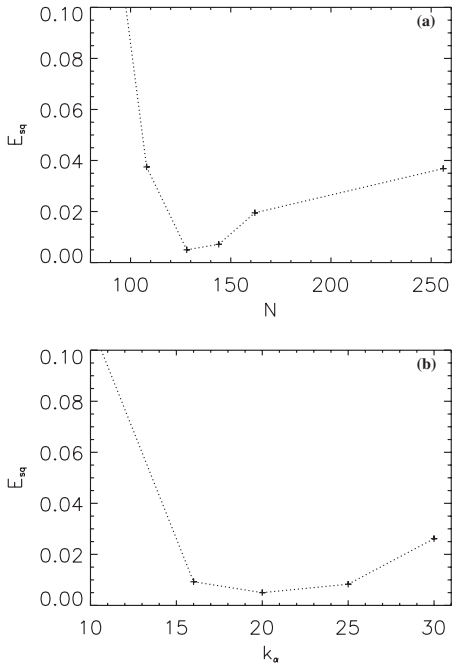

FIG. 10. Plots for Re≈670 simulations. (a) Error [see Eq. (25)] versus simulation resolution for $k_\alpha=20$. The optimal (grid-dependent) LES is for a resolution of $N\approx128$ and has a much smaller error compared to the DNS than the grid-independent LANS α solution at higher resolution. (b) Error versus k_α for $N=128$. At a given resolution the optimal value for α is not zero but occurs at a local minimal error. Any $k_\alpha\in[15,25]$ has an error near the minimum, indicating that a LES solution may perform well for a range of parameters near the optimal ones. A constant of $C=C_0\mathrm{Re}^{1/2}\approx47$ in Eq. (22) is found to correspond with optimal α LES approximations.

full Navier-Stokes equations. Due to these errors being, in some sense, in opposition, the optimal α LES solution is found at a lower resolution than the grid-independent solution. Indeed, we see by examining Fig. 10(a) that for a given filter the combination of truncation error and the LANS α solution is a better approximation to the DNS. For fixed resolution, Fig. 10(b), the optimal value for α is not zero but has some finite value. This local minimum error shown in the figure keeps α from going to zero ($k_\alpha\to\infty$) in dynamical models [15]. We also note, that the error is low for a finite range of N and k_α near the minimum, indicating that an α LES solution may perform well for a range of parameters near the optimal ones. We find the resolution for an optimal α LES is also predicted by Eq. (22) (with $C\approx47$ for Re ≈670, or $C_0\approx1.8$). That is, the optimal α LES resolution is just below that for grid-independent LANS α solutions. Having demonstrated the predictability of the resolution for grid-independent LANS α and of LANS α LES given a Reynolds number and a filter, in the following section we seek to determine sufficient conditions on the free parameter α for the LANS α model to be a successful LES.

A. Free parameter α and quality of the α LES

In this section, we make an analysis of the LES potential of the LANS α simulation by considering only the grid-

independent LANS α solutions identified using Eq. (22). Note that, from the results discussed in the previous section, we expect LANS α optimal grid-dependent α LES approximations to have better performance. In the limit of α going to zero, LANS α Eq. (2) recovers the Navier-Stokes equations, Eqs. (1), but the question we address now is how small must α be for LANS α solutions to be good approximations to Navier-Stokes solutions. There are several length scales that α could be related to: the forcing scale l_F, the integral scale $L=2\pi\int_0^\infty E(k)k^{-1}dk/\int_0^\infty E(k)dk$, the Taylor microscale λ, or the Kolmogorov dissipation scale η_K. Plots of the mean square spectral errors compared to DNS [see Eq. (25)] versus these scales are shown in Fig. 11. While the general trend of errors decreasing with α is apparent in all cases, in Fig. 11(a) we see a large difference between errors at varying Reynolds numbers and similar ratios of α to the forcing scale l_F. For a linear least-squares fit, the goodness of fit, $\chi^2 \equiv \Sigma(E_{\mathrm{sq}}^{\mathrm{actual}} - E_{\mathrm{sq}}^{\mathrm{fit}})^2$ was found to be $\chi^2=6.2\times10^{-2}$. The errors for Re $\approx$3300 are much larger than for the same ratio l_F/α as results at both Re$\approx$500 and Re$\approx$670. This is also the case for the integral scale. However, the quality of the α LES appears to be closely tied to the ratio of α to the Kolmogorov dissipation scale. In Fig. 11(b) the errors are plotted versus the ratio of the dissipation scale η_K to α. We see a very strong dependence ($\chi^2=2.5\times10^{-2}$) between errors for several runs with four different Reynolds numbers, indicating that the quality of the LANS α LES approximation is a function of the ratio of α to the dissipative scale. Finally, in Fig. 11(c) the errors are plotted versus the ratio of the Taylor scale, λ, to α. We find $\chi^2=3.1\times10^{-2}$ for a linear least-squares fit. We note that a single experiment conducted at Re$\approx$8300 (the asterisk) confirms that the maximal value of α is tied to the dissipation scale and not the Taylor scale. This is more clearly demonstrated in Fig. 12 where we plot compensated energy spectra for a nearly constant ratio λ/α at three Reynolds numbers. We see that the maximum deviation from the DNS spectrum increases with Re. As λ/α is the same in all cases, the optimal α is not dependent on the Taylor scale.

These findings were not accessible at lower Reynolds numbers due to inadequate separation of scales. For example, we give in Fig. 13(a) spectral flux for DNS at Re $\approx$500, 670, and 3300, respectively. We define the kinetic energy transfer function $T(k)$ in Fourier space as $T(k)=-\int\hat{\mathbf{v}}_k\cdot\widehat{(\boldsymbol{\omega}\times\mathbf{v})}dV$, where $\hat{(\cdot)}$ represents the Fourier transform. For the LANS α model we have $T_\alpha(k)=-\int\tilde{\mathbf{v}}_k\cdot\widehat{(\boldsymbol{\omega}\times\mathbf{u})}dV$ where $\boldsymbol{\omega}=\nabla\times\mathbf{v}$. The flux is defined as usual from the transfer function as

$$\Pi_{(\alpha)}(k) = \int_0^k T_{(\alpha)}(k')dk'. \tag{26}$$

Only Re$\approx$3300 (and Re$\approx$8300 not pictured here) demonstrates a range of nearly constant flux (a well-defined inertial range) before the dissipation scales. Following the scaling arguments in Ref. [11], one effect of the α model is to increase the time scale for the cascade of energy to small scales. This reduces the flux as α increases (k_α decreases) as do the hypothesized rigid bodies; this can be seen in Fig. 13(b). (Note that in a DNS at high resolution, 80% of the flux is from local interactions, which are strongly suppressed at scales smaller than α [21].) As dissipation dominates the flux for low and moderate Reynolds number, the reduced flux of the α model has little consequence for these simulations. With a substantial inertial range, however, this reduced flux results in a pileup of energy for scales larger than the dissipative scale and the spectrum approaches the k^1 spectrum discussed in Sec. III. As a consequence of the integral conservation of energy ($E_\alpha=\int\mathbf{u}\cdot\mathbf{v}$) there is a corresponding decrease of energy at large scales. Consequently, as the inertial range increases, α must be moved to smaller and smaller scales in order for the LANS α simulation not to alter scales

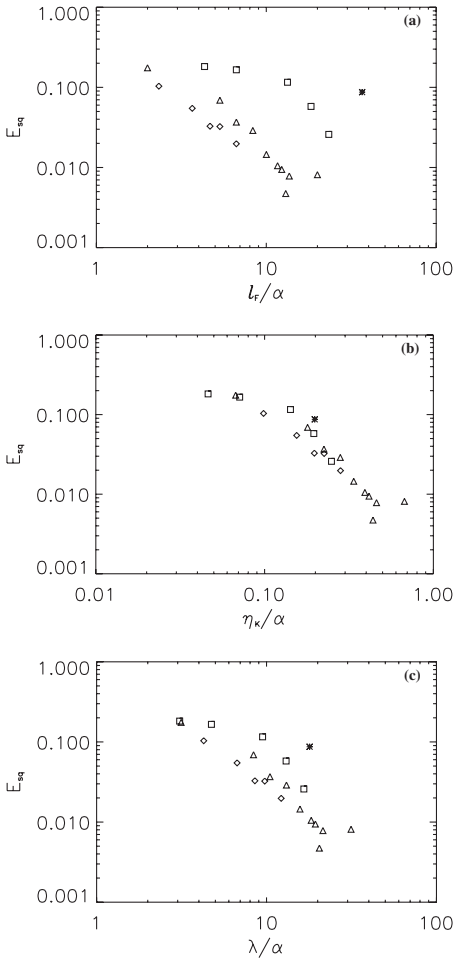

FIG. 11. Plot of errors, Eq. (25), of grid-independent solutions compared to DNS. Asterisks are for Re$\approx$8300, squares for Re $\approx$3300, triangles for Re$\approx$670, and diamonds for Re$\approx$500. The single right-most triangle in all plots corresponds to a value of α in the dissipative range (k_α=60). The norm we employ to measure the error, Eq. (25), is no longer a good norm when dissipative scales are considered. (a) Errors versus l_F/α. No clear correlation between LES quality and the ratio of the forcing scale to α holds independently of Reynolds numbers. (b) Errors versus ratio of dissipative scale, η_K, to α. The quality of the LES appears to be closely tied to this ratio. (c) Errors versus ratio of Taylor wave number λ to α. The Re$\approx$8300 experiment (asterisk) indicates that the quality of the α LES is not tied to the Taylor scale.

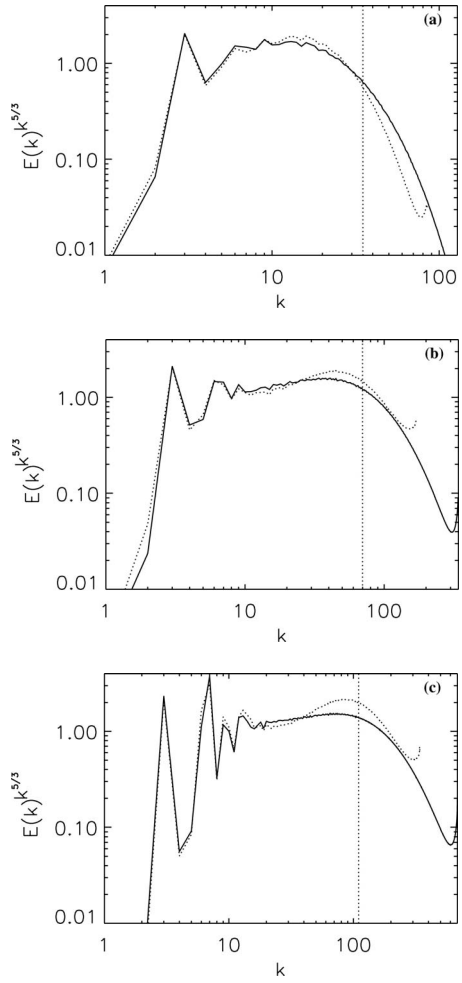

FIG. 12. Compensated averaged grid-independent energy spectra for DNS (solid) and LANS α results (dotted) holding the ratio of Taylor scale λ to α nearly constant. Vertical dotted lines indicate k_α. (a) Re$\approx$670 and k_α=35 (λ/α=18). (b) Re$\approx$3300 and k_α=70 (λ/α=17). (c) Re$\approx$8300 and k_α=110 (λ/α=17). We see that the maximum deviation from the DNS increases with Re. This is due to the greater distance between α and the dissipative scale η_K. (Note that scales larger than k=3 are affected by numerical truncation issues.)

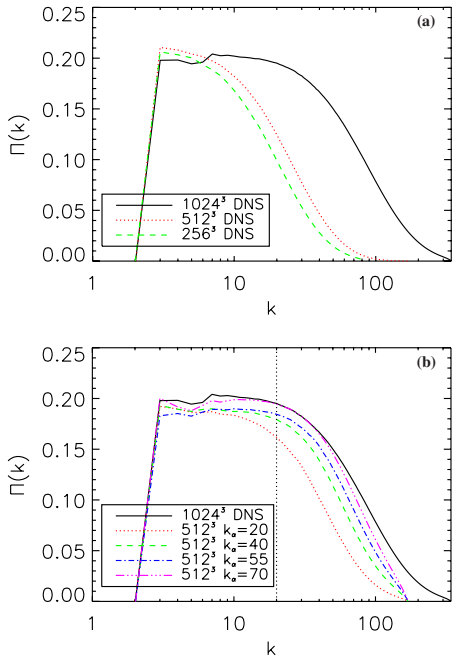

FIG. 13. (Color online) (a) Energy flux, Eq. (26), for three DNSs with Re$\approx$3300 (black, solid), Re$\approx$670 (red, dotted), and Re$\approx$500 (green, dashed). No inertial range is discernible in the flux functions except for the highest-Reynolds-number case. The initial plateau followed by a bump and another plateau (for the case at the highest Reynolds number) is a result of the forcing employed. (b) Energy flux at Re$\approx$3300 for both DNS and α model runs; DNS is the black, solid line. See inset for LANS α parameters. The LANS α model gives a reduced flux, which is linked to the significant pileup of energy at high wave number as visible in the energy spectrum (see Fig. 14). Plots of ε_α versus t (not shown) also show that flux decreases (on average, at long times) with increasing α.

larger than α. In summary, the α model's reduced flux of energy to small scales is more crucial when the dissipation scale is farther away from α.

B. Numerical savings from employing the LANS α model

If α must be directly proportional to the Kolmogorov dissipation scale, we can estimate the LES computational savings of the LANS α model. For the Navier-Stokes equations we have $n_{\mathrm{DOF(NS)}} \propto \mathrm{Re}^{9/4}$ and, as we verified in Sec. IV, for the LANS α model we have $n_{\mathrm{DOF}(\alpha)} = C_0^3 k_\alpha \mathrm{Re}^{3/2}/27$. If k_α is directly proportional to the Navier-Stokes dissipation wave number k_η, we arrive at

$$k_\alpha \approx \frac{1}{4} k_\eta \propto \mathrm{Re}^{3/4}, \tag{27}$$

and, consequently,

$$n_{\mathrm{DOF}(\alpha)}^{\mathrm{LES}} \propto Re^{9/4}. \tag{28}$$

Note that, for free α, $n_{\mathrm{DOF}(\alpha)}$ (the DOF of the LANS α model) is much smaller than $n_{\mathrm{DOF(NS)}}$. But, to obtain an optimal LES, α is tied to k_η; then the resolution requirements ($n_{\mathrm{DOF}(\alpha)}^{\mathrm{LES}}$) are different and the decrease in necessary computational resolution from employing the LANS α method is fixed. In fact, for the forcing and boundary conditions employed, we find

$$n_{\mathrm{DOF}(\alpha)}^{\mathrm{LES}} \approx \frac{1}{12} n_{\mathrm{DOF(NS)}} \tag{29}$$

We note that Eq. (28) is consistent with theoretical predictions given in Ref. [20]. Other LESs such as the similarity model [43] and the nonlinear (or gradient) model [44,45] have also exhibited the characteristic that they achieve only moderate reductions in resolution and are, therefore, frequently used in mixed models with a Smagorinsky term (see, e.g., [3]). That such additional terms will be required for the LANS α method to reproduce the energy spectrum of high-Re flows, may not be a significant factor in its usability. Note that the usual addition of extra dissipative subgrid-stress terms (as in the Smagorinsky model) also introduces a

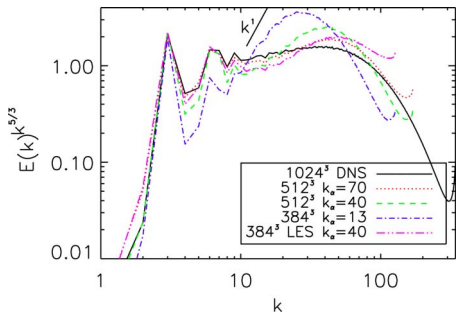

FIG. 14. (Color online) Compensated energy spectra averaged over $t \in [8,9]$, Re$\approx$3300. DNS is the solid black line and grid-independent LANS α solutions are shown as (red online) dotted (k_α=70), (green) dashed (k_α=40), and (blue) dash-dotted (k_α=13) lines, respectively. A single LANS α LES is shown as a (pink) dash-triple-dotted line (k_α=40, N=384). The LES is seen to better approximate the DNS spectrum than the grid-independent solution for the same value of α ($2\pi/40$). As α is increased the energy spectrum approaches the k^1 spectrum discussed in Sec. III B.

stronger dependence of the system of equations on the spatial resolution, since the filter width in such models is often associated with the maximum wave number in the box, $k_{\max}$. In that case, it can make more sense to use grid-dependent solutions of LANS α (discussed at the beginning of Sec. V) which give an optimal LANS α LES, and can as a result give an extra gain in the computational costs.

We also conclude that, with the scale α being tied to the dissipation scale η_K, the LANS α model behaves more like a quasi-DNS by opposition to a traditional LES. Note, however, that a factor of $\approx$2.3 in resolution gain translates into a factor 27 in CPU time and a factor 12 in memory savings, still a substantial gain.

VI. LANS α MODEL AT VERY HIGH REYNOLDS NUMBER

In this section, we compare and contrast LANS α and Navier-Stokes solutions at high Reynolds number. Using results of previous sections for optimal resolution and the necessary value of α to approximate DNS, we now evaluate both grid-independent LANS α solutions and a single LANS α LES for a highly turbulent flow (Re$\approx$3300, $R_\lambda \approx 790$). We calculate grid-independent solutions for k_α=70 (N=512), for k_α=40 (N=512), and for k_α=13 (N=384). A LANS α LES solution is computed for k_α=40 (N=384). Averaged compensated energy spectra are shown in Fig. 14. We see that the optimal LANS α LES is a better approximation of the DNS spectra than the grid-independent LANS α result for the same value of α ($2\pi/40$). We also see that, if α is increased further, the energy spectrum approaches the k^1 spectrum discussed in Sec. III B.

Figure 15 is a perspective volume rendering of the enstrophy density ω^2 ($\boldsymbol{\omega}\cdot\bar{\boldsymbol{\omega}}$ for LANS α) for the DNS, k_α=70 LANS α, and k_α=13 LANS α simulations. Due to the late time depicted here (t=9, longer than a Lyapunov time) there can be no point-by-point comparison between the simulations. However, we note that the helical structure of the vortex tubes is preserved by the α model but that the tubes themselves are shorter and somewhat thicker for large values of α. As was noted for moderate Reynolds numbers, this is due to the LANS α method suppressing vortex stretching dynamics without changing its qualitative features [9]. This is in contrast to 2D LANS α results, where the vorticity structures are seen to get thinner as α increases [36]. This could also be related to the scaling differences between 2D and 3D LANS α models. It has been claimed that the development of helical structures in turbulent flows can lead to the depletion of nonlinearity and the quenching of local interactions [46,47]. The depletion of energy transfer due to local interactions at some cutoff in wave number is also believed to bring about the bottleneck effect [22,48–50]. Consistent with these results, in the 2D LANS α results (where the vorticity structures are finer than Navier-Stokes) the spectrum is steeper, and in the 3D LANS α results (where the

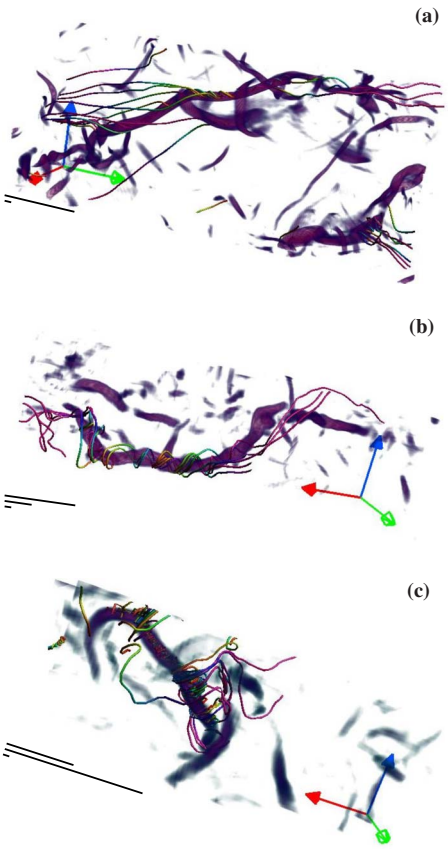

FIG. 15. (Color online) Rendering of enstrophy density ω^2 ($\boldsymbol{\omega}\cdot\bar{\boldsymbol{\omega}}$ for LANS α model). Due to the late time depicted here (t=9, longer than a Lyapunov time) there can be no point-by-point comparison between the simulations. Instead, regions with approximately the same dimensions are selected around vortex tubes. Velocity **v** field lines are also shown illustrating the helical nature of the tubes, which is seen to be captured by the LANS α simulation. (a) DNS. The thick bars represent, from top to bottom, the Taylor scale λ and the dissipative scale η_K, respectively. For LANS α results the scale α is depicted between these two. (b) k_α=70, N=512. (c) k_α=13, N=384. We see that, for large values of α, the vortex tubes become shorter and somewhat thicker.

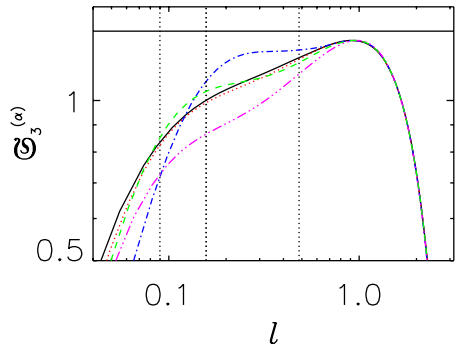

FIG. 16. (Color online) Compensated third-order structure function versus length l (a horizontal line scales with l). Structure functions corresponding to the Kármán-Howarth theorem are depicted [$\mathfrak{S}_3$ for DNS, $\mathfrak{S}_3^\alpha \equiv \langle(\delta u)^2 \delta v\rangle$ for LANS α]. Labels are as in Fig. 14. The dotted vertical lines indicate the various α's. A small inertial range for the DNS near $l=1$ is reproduced by the LANS α simulation. The largest α $(2\pi/13)$ exhibits a second inertial range at scales just smaller than α [$\langle(\delta u)^2 \delta v\rangle \sim l$ is consistent with Eq. (15)].

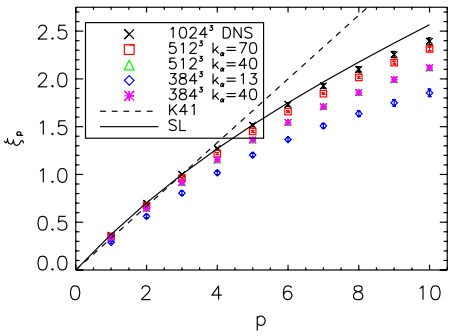

FIG. 17. (Color online) Structure function scaling exponent ξ_p versus order p. Black ×'s are shown for the DNS. Grid-independent LANS α results are shown as (red online) boxes ($k_\alpha=70$), as (green) triangles ($k_\alpha=40$), and as (blue) diamonds ($k_\alpha=13$). LANS α LES ($k_\alpha=40$, $N=384$) is shown as (pink) asterisks. The dashed line indicates K41 scaling and the solid line the She-Lévêque (SL) formula [56].

vorticity structures are shorter but fatter than Navier-Stokes), the spectrum is shallower.

Figure 16 shows the third-order (mixed) structure functions corresponding to the Kármán-Howarth theorems versus length l. For the DNS, we show $\mathfrak{S}_3 \equiv \langle \delta v^3 \rangle$ and $\mathfrak{S}_3^\alpha \equiv \langle(\delta u)^2 \delta v\rangle$ for the LANS α model. The dotted vertical lines indicate the various α's. A small inertial range for the DNS near $l=1$ is reproduced by all LANS α results. The largest α $(2\pi/13)$ exhibits a second inertial range at scales just smaller than α [$\langle(\delta u)^2 \delta v\rangle \sim l$ is consistent with Eq. (15)]. We note this is the first demonstration of third-order structure functions in the LANS α results consistent with a K41 inertial range followed by an α inertial range and finally a dissipative range. Next, we observe the scaling of the longitudinal structure functions,

$$S_p(l) \equiv \langle |\delta v_\parallel|^p \rangle, \tag{30}$$

where we again substitute the H^1_α norm for the L^2 norm in the case of LANS α,

$$S_p^\alpha(l) \equiv \langle |\delta u_\parallel \delta v_\parallel|^{p/2} \rangle. \tag{31}$$

We utilize the extended self-similarity (ESS) hypothesis [51–53] which proposes the scaling

$$S_p(l) \propto S_3(l)^{\xi_p} \tag{32}$$

or, for the LANS α model,

$$S_p^\alpha(l) \propto \langle(\delta u)^2 \delta v\rangle^{\xi_p}. \tag{33}$$

We display our results in Fig. 17. We note that, for the LANS α results, the third-order exponent is not equal to unity, in contrast to the Navier-Stokes case. The Kármán-Howarth theorem implies that $\langle(\delta u)^2 \delta v\rangle \sim l$, not $S_3^\alpha(l) \sim l$. We measured the deviation from linearity for each experiment (not depicted here) and found that the LANS α model becomes more intermittent as α increases ($k_\alpha=13$ is slightly more intermittent than the DNS). As artificially dropping the local small-scale interactions gives enhanced intermittency [54,55], this increased intermittency is the expected result of the LANS α model reducing interactions at scales smaller than α. We note, however, that even with such a large filter, the LANS α simulation is a good approximation to the intermittency properties of the DNS. This is surprising given its energy spectrum and reduced flux in the inertial range. It is probably linked to the fact that the LANS α method preserves global properties (in an H^1 sense) of the Navier-Stokes equations and that these properties are important to the dynamics of small scales as measured by high-order structure functions.

VII. CONCLUSIONS

We computed solutions of the Lagrangian-averaged Navier-Stokes α model in three dimensions for significantly higher Reynolds numbers (up to $\mathrm{Re} \approx 8300$) than have previously been accomplished, and performed numerous forced turbulence simulations of the LANS α equations to study their equilibrium states. The results were compared to DNSs for $\mathrm{Re} \approx 500$, 670, 3300, and 8300, the last performed on a grid of 2048^3 points. We note that there are two ways to view the LANS α simulations: as converged or "grid-independent" solutions of the LANS α equations or as large eddy simulations (α LESs) that include grid effects. We found a definite difference between the two approaches in that the fully converged grid-independent LANS α method is not the best approximation to a DNS of the Navier-Stokes equations. Instead, the minimum error is a balance between truncation errors and the approximation error due to using the LANS α instead of the full Navier-Stokes equations. Because these errors are, in some sense, in opposition, the optimal α LES solution was found at a lower resolution than the grid-independent solution (the error was low for a finite range of N and α near the minimum, indicating that a LANS α simulation viewed as a LES solution may perform well for a range of parameters). Unlike the 2D case [36], the 3D LANS α has been shown to be a subgrid model (i.e., it reduces the resolution requirements of a given computation).

This difference between 2D and 3D LANS α methods indicates that other α models [like the Lagrangian-averaged magneto-hydrodynamics alpha (LAMHD α) [57,58] or the barotropic vorticity alpha (BV α) equations [42]] may behave differently, and studies of these systems at high resolution may be required.

We confirm the presence of the theoretically predicted l^3 scaling of the third-order structure function (corresponding to a k^{-1} scaling of the energy spectrum) [11,16,37] through its bound on the number of degrees of freedom for the LANS α model [11], in the structure functions of the smoothed velocity in simulations with large α, and in the spectrum of specific spatial portions of the flow. In so doing, we have validated the predictive power of the bound $n_{\mathrm{DOF}(\alpha)} < \mathcal{C}\alpha^{-1}\,\mathrm{Re}^{3/2}$ for the numerical resolution for grid-independent LANS α solutions and for optimal LANS α LES (with a separate constant of proportionality). The great utility of the prediction is that the single constant can be determined cheaply at low and moderate Reynolds numbers and predicts the resolution requirement for the highest Reynolds numbers attainable. We further found no great change in this single constant when employing the nonhelical Taylor-Green or the maximally helical ABC forcings.

However, the small-scale ($k\alpha \gg 1$) LANS α spectrum was observed to be k^{+1}. We attribute this to the frozen-in-turbulence closure employed in deriving the α model. For scales smaller than α, portions of the smoothed flow $\mathbf{u}$ are locked into rigid bodies. By "rigid bodies," we mean that the internal degrees of freedom are frozen and these portions give no contribution to the energy cascade. This is consistent both with the observed k^{+1} spectrum and with field increments $\delta u_{\parallel}$ being observed to be approximately zero over a large portion (compared to Navier-Stokes) of the flow. The turbulent energy cascade occurs in the space between these rigid portions. While the k^{-1} portions are subdominant to the k^{+1} portions in the energy spectrum, they prevail in the cascade and hence in both the structure functions and the degrees of freedom of the LANS α attractor.

We find that both of these scalings (k^{+1} and k^{-1}) contribute to a reduction of flux at constant energy (i.e., the dissipation is reduced as has previously been observed in 2D calculations [59]). This leads to a shallower (or even growing) energy spectrum as α increases. Thus, for the LANS α method viewed as a LES to reproduce the Navier-Stokes energy spectrum, it is necessary that α be not much larger than the dissipation scale ($\alpha \lessapprox 4\eta_K$ independent of Reynolds number); in that sense, it can be considered as a quasi-DNS as opposed to a traditional LES, substantially larger Reynolds numbers being modeled in the latter case, leading to substantially larger gain in resolution. As a consequence, the computational savings of the LANS α approach is fixed and not a function of Reynolds number. (However, and unlike the 2D case, the 3D α model does give a computational saving when used as a LES.) This result was not accessible at lower Reynolds numbers due to inadequate separation of scales. However, in one previous study for decaying turbulence with energy initially mostly at low wave numbers ($k=3$), it was evident that as time evolved and energy moved to smaller scales, the resolution requirements of the LANS α model increased [17]. Other LESs such as the similarity model [43] and the nonlinear (or gradient) model [44,45] have also exhibited the characteristic that resolution may be decreased only modestly and are, therefore, frequently used in mixed models with a Smagorinsky term (see, e.g., [3]). That such additional terms will be required for the LANS α method to reproduce the energy spectrum of high-Re flows may not be a significant factor in its usability.

We compared and contrasted the LANS α simulation to a DNS at $\mathrm{Re} \approx 3300$, considering both structures and high-order statistics such as the longitudinal structure functions, which are related to intermittency. With an appropriate choice of α we were able to observe a Navier-Stokes inertial range followed by a LANS α inertial range at scales smaller than α. For this second inertial range we again observed a k^{+1} energy spectrum. As α increased, we noted a change in the aspect ratio of vortex tubes (they became shorter and fatter). This can be related to quenching of local small-scale interactions at scales smaller than α and, thus, to the shallower spectrum for the 3D LANS α results [46–50,22]. Therefore, in the 2D LANS α method (where the vorticity structures are finer than in the Navier-Stokes equations), the spectrum is steeper [36] and in the 3D LANS α method (where the vorticity structures are shorter but fatter than in the Navier-Stokes results), the spectrum is shallower. Finally, an examination of the longitudinal structure functions indicate that intermittency is increased as the parameter α is increased consistent with the suppression of local small-scale interactions at scales smaller than α [54,55].

The elimination of the faster and faster interactions among smaller and smaller scales through the modified nonlinearity in the LANS α method (together with the discrepancy between its solutions and Navier-Stokes solutions) highlights the importance of these interactions down to scales only slightly larger than the dissipative scale. That is, by removing these interactions anywhere in the inertial range (e.g., $\alpha \gtrapprox 4\eta_K$), the resulting energy spectrum was found to differ from the DNS at scales larger than α. The intermittency properties of the DNS, however, were well reproduced even with large filters. Noting this, if the LANS α method's k^1 energy spectrum is not important for a given application, much greater reductions in resolution can be achieved. Future work should address whether this may be remedied in a LANS α LES by the inclusion of another (dissipative) model for these interactions, or (in the case of magnetohydrodynamics [57,58]) whether this problem is less significant because of the presence of greater spectral nonlocality [60–62]. The effect of the LANS α method on the detailed scale-by-scale energy transfer should also be investigated as our results indicate that a model for local small-scale interactions would improve the α model. Another direction of future research is to explore other reduced LANS α models, the Clark α and Leray α models, which break the frozen-in-turbulence closure and also the conservation of circulation. Finally, note that, because of its greater mathematical tractability, the LANS α model possibly allows for a better understanding of multiscale interactions in turbulent flows thus modeled; therefore, detailed studies such as the one presented here may, in fine, allow for a better understanding of turbulence itself.

ACKNOWLEDGMENTS

Computer time was provided by NCAR and by the National Science Foundation Terascale Computing System at the Pittsburgh Supercomputing Center. The NSF Grant No. CMG-0327888 at NCAR supported this work in part and is gratefully acknowledged. Three-dimensional visualizations of the flows were done using VAPOR. The authors would like to express their gratitude for valuable discussions with Bob Kerr. The National Center for Atmospheric Research is sponsored by the National Science Foundation.

[1] P. J. Mason, Q. J. R. Meteorol. Soc. **120**, 1 (1994).
[2] M. Lesieur and O. Metais, Annu. Rev. Fluid Mech. **28**, 45 (1996).
[3] C. Meneveau and J. Katz, Annu. Rev. Fluid Mech. **32**, 1 (2000).
[4] J. R. Kulkarni, L. K. Sadani, and B. S. Murthy, Boundary-Layer Meteorol. **90**, 217 (1999).
[5] G. Heinemann, Theor. Appl. Climatol. **83**, 35 (2006).
[6] D. D. Holm, J. E. Marsden, and T. S. Ratiu, Adv. Math. **137**, 1 (1998).
[7] S. Chen, C. Foias, D. D. Holm, E. Olson, E. S. Titi, and S. Wynne, Phys. Rev. Lett. **81**, 5338 (1998).
[8] S. Chen, C. Foias, D. D. Holm, E. Olson, E. S. Titi, and S. Wynne, Physica D **133**, 49 (1999).
[9] S. Chen, D. D. Holm, L. G. Margolin, and R. Zhang, Physica D **133**, 66 (1999).
[10] S. Chen, C. Foias, D. D. Holm, E. Olson, E. S. Titi, and S. Wynne, Phys. Fluids **11**, 2343 (1999).
[11] C. Foias, D. D. Holm, and E. S. Titi, Physica D **152-153**, 505 (2001).
[12] D. D. Holm, J. E. Marsden, and T. S. Ratiu, Phys. Rev. Lett. **80**, 4173 (1998).
[13] D. D. Holm, Chaos **12**, 518 (2002).
[14] D. D. Holm, Physica D **170**, 253 (2002).
[15] H. Zhao and K. Mohseni, Phys. Fluids **17**, 075106 (2005).
[16] A. Cheskidov, D. D. Holm, E. Olson, and E. S. Titi, Proc. R. Soc. London, Ser. A **461**, 629 (2005).
[17] K. Mohseni, B. Kosović, S. Shkoller, and J. E. Marsden, Phys. Fluids **15**, 524 (2003).
[18] B. J. Geurts and D. D. Holm, in *Turbulent Flow Computation*, edited by D. Drikakis and B. J. Geurts (Kluwer Academic Publishers, London, 2002), p. 237.
[19] B. J. Geurts and D. D. Holm, J. Turbul. **7**, 1 (2006).
[20] J. D. Gibbon and D. D. Holm, Physica D **220**, 69 (2006).
[21] A. Alexakis, P. D. Mininni, and A. Pouquet, Phys. Rev. Lett. **95**, 264503 (2005).
[22] P. D. Mininni, A. Alexakis, and A. Pouquet, Phys. Rev. E **74**, 016303 (2006).
[23] D. O. Gómez, P. D. Mininni, and P. Dmitruk, Phys. Scr. **116**, 123 (2005).
[24] D. O. Gómez, P. D. Mininni, and P. Dmitruk, Adv. Space Res. **35**, 899 (2005).
[25] G. I. Taylor and A. E. Green, Proc. R. Soc. London, Ser. A **158**, 499 (1937).
[26] P. D. Mininni, Y. Ponty, D. C. Montgomery, J.-F. Pinton, H. Politano, and A. Pouquet, Astrophys. J. **626**, 853 (2005).
[27] M. Brachet, C. R. Acad. Sci., Ser. II: Mech. **311**, 775 (1990).
[28] Y. Ponty, P. D. Mininni, D. C. Montgomery, J.-F. Pinton, H. Politano, and A. Pouquet, Phys. Rev. Lett. **94**, 164502 (2005).
[29] T. de Kármán and L. Howarth, Proc. R. Soc. London, Ser. A **164**, 192 (1938).
[30] D. D. Holm, J. Fluid Mech. **467**, 205 (2002).
[31] U. Frisch, *Turbulence, The Legacy of A. N. Kolmogorov* (Cambridge University Press, Cambridge, U.K., 1995).
[32] A. N. Kolmogorov, Dokl. Akad. Nauk SSSR **30**, 299 (1941), reprinted in Proc. R. Soc. London, Ser. A **434**, 9 (1991).
[33] A. N. Kolmogorov, Dokl. Akad. Nauk SSSR **31**, 538 (1941).
[34] A. N. Kolmogorov, Dokl. Akad. Nauk SSSR **32**, 16 (1941), reprinted in Proc. R. Soc. London, Ser. A **434**, 15 (1991).
[35] R. H. Kraichnan, Phys. Fluids **10**, 1417 (1967).
[36] E. Lunasin, S. Kurien, M. Taylor, and E. Titi, e-print arXiv:physics/0702196.
[37] C. Cao, D. D. Holm, and E. S. Titi, J. Turbul. **6**, 19 (2005).
[38] A. A. Ilyin, E. M. Lunasin, and E. S. Titi, Nonlinearity **19**, 879 (2006).
[39] C. Cichowlas, P. Bonaïti, F. Debbasch, and M. Brachet, Phys. Rev. Lett. **95**, 264502 (2005).
[40] B. J. Geurts and J. Fröhlich, Phys. Fluids **14**, L41 (2002).
[41] J. Meyers, B. J. Geurts, and M. Baelmans, Phys. Fluids **15**, 2740 (2003).
[42] D. D. Holm and B. Nadiga, J. Phys. Oceanogr. **33**, 2355 (2003).
[43] *Improved Subgrid-Scale Models for Large-Eddy Simulation*, edited by J. Bardina, J. H. Ferziger, and W. C. Reynolds, American Institute of Aeronautics and Astronautics, Fluid and Plasma Dynamics Conference, 13th, Snowmass, Colorado (1980), p. 10.
[44] A. Leonard, in *Turbulent Diffusion in Environmental Pollution*, Proceedings of the Second Symposium, Charlottesville, VA, 1973, Vol. A (Academic, New York, 1974), pp. 237–248.
[45] R. A. Clark, J. H. Ferziger, and W. C. Reynolds, J. Fluid Mech. **91**, 1 (1979).
[46] H. K. Moffatt and A. Tsinober, Annu. Rev. Fluid Mech. **24**, 281 (1992).
[47] A. Tsinober, *An Informal Introduction to Turbulence* (Kluwer, Dordrecht, 2001).
[48] J. R. Herring, D. Schertzer, M. Lesieur, G. R. Newman, J. P. Chollet, and M. Larcheveque, J. Fluid Mech. **124**, 411 (1982).
[49] D. Lohse and A. Müller-Groeling, Phys. Rev. Lett. **74**, 1747 (1995).
[50] D. O. Martínez, S. Chen, G. D. Doolen, R. H. Kraichnan, L.-P. Wang, and Y. Zhou, J. Plasma Phys. **57**, 195 (1997).
[51] R. Benzi, S. Ciliberto, C. Baudet, G. Ruiz Chavarria, and R. Tripiccione, Europhys. Lett. **24**, 275 (1993).
[52] R. Benzi, S. Ciliberto, R. Tripiccione, C. Baudet, F. Massaioli, and S. Succi, Phys. Rev. E **48**, R29 (1993).
[53] R. Benzi, L. Biferale, S. Ciliberto, M. V. Struglia, and R. Tripiccione, Phys. Rev. E **53**, R3025 (1996).

[54] J.-P. Laval, B. Dubrulle, and S. Nazarenko, Phys. Fluids **13**, 1995 (2001).
[55] B. Dubrulle, J.-P. Laval, S. Nazarenko, and O. Zaboronski, J. Fluid Mech. **520**, 1 (2004).
[56] Z. S. She and E. Lévêque, Phys. Rev. Lett. **72**, 336 (1994).
[57] J. P. Graham, P. D. Mininni, and A. Pouquet, Phys. Rev. E **72**, 045301(R) (2005).
[58] J. P. Graham, D. D. Holm, P. Mininni, and A. Pouquet, Phys. Fluids **18**, 045106 (2006).
[59] D. Biskamp and E. Schwarz, Phys. Plasmas **8**, 3282 (2001).
[60] A. Alexakis, P. D. Mininni, and A. Pouquet, Phys. Rev. E **72**, 046301 (2005).
[61] P. Mininni, A. Alexakis, and A. Pouquet, Phys. Rev. E **72**, 046302 (2005).
[62] A. Alexakis, P. D. Mininni, and A. Pouquet, Astrophys. J. **640**, 335 (2006).